

# Pressure Transport in DNS of Turbulent Natural Convection in Horizontal Fluid Layers

M. Wörner and G. Grötzbach

*Forschungszentrum Karlsruhe, IRS, Karlsruhe, Germany*

**Abstract** — Direct numerical simulation data of two types of turbulent natural convection in horizontal fluid layers are used to compute turbulent diffusive transport terms for turbulence kinetic energy and vertical turbulent heat flux. For both quantities turbulent diffusive transport is represented by a pressure correlation and a triple correlation. While for Rayleigh-Bénard convection in air the pressure correlation dominates the triple correlation, for the convection in an internally heated layer the opposite behaviour is observed. The dominance of pressure transport in the Rayleigh-Bénard convection and its minor importance in the internally heated layer is explained by the coherent structures and dynamics of the respective flow. The coherent structures are intermittent and exist only for short time intervals. Thus, conventional closure relations for turbulent diffusive transport, which are used in statistical turbulence models based on long-time averaged quantities, may not be appropriate for the flows under consideration.

## 1. Introduction

To calculate turbulent flow and heat transfer, in second-order statistical turbulence models balance equations are solved for characteristic turbulent quantities such as the turbulence kinetic energy, its dissipation rate, the Reynolds stresses, the turbulent heat fluxes, and temperature variance. The balance equations actually solved are derived from analytical equations by introducing simplifications and model assumptions. In each analytical balance equation, terms can be classified in the categories: (1) rate of change, (2) convective transport, (3) production  $P$ , (4) sink  $S$ , and (5) diffusive transport  $D$ .

In fully developed natural convection where no mean flow through the channel is present, e.g. in the classical Rayleigh-Bénard convection in the fully turbulent regime, terms (1) and (2) drop out when averages are taken over long times. The balance equation for a general turbulent quantity  $\phi$  then simplifies to

$$P_\phi + S_\phi + D_\phi = 0. \quad (1)$$

In a state of local equilibrium, the local production and sink of a quantity  $\phi$  are in balance, thus  $P_\phi = S_\phi$  and  $D_\phi = 0$ . However, in many situations  $\phi$  is mainly produced in the center of the flow domain, while the sink term is maximum near walls. Thus, there is no local equilibrium and the diffusive transport is important, as it redistributes  $\phi$  across the flow domain. In such situations, accurate modelling of the turbulent part of diffusive transport  $D_{\phi,turb}$  is of special significance.

In this paper, we focus our attention on the balance equations for turbulence kinetic energy  $k = \frac{1}{2}\overline{u'_i u'_i} = \frac{1}{2}(\overline{u'_1 u'_1} + \overline{u'_2 u'_2} + \overline{u'_3 u'_3})$  and turbulent heat fluxes  $q_i = \overline{u'_i T'}$ . Using non-dimensional variables (see section 2), the turbulent diffusive transport is represented by the correlations

$$D_{k,turb} = -\frac{\partial}{\partial x_j} \left( \frac{1}{2} \overline{u'_j u'_i u'_i} + \overline{u'_j p'} \right) \quad (2)$$

and

$$D_{q_i,turb} = -\frac{\partial}{\partial x_j} \left( \overline{u'_i u'_j T'} + \delta_{ij} \overline{T' p'} \right). \quad (3)$$

Thus, velocity and pressure fluctuations contribute to  $D_{k,turb}$  and velocity, pressure and temperature fluctuations to  $D_{q_i,turb}$ .

Modelling the pressure transport is particularly difficult, because pressure fluctuations within a turbulent flow are one of the Great “Unmeasurables” [1]. Lumley [2] suggested to account for the pressure transport of  $k$  by

$$\overline{u'_j p'} = -\frac{1}{5} \overline{u'_j u'_i u'_i}. \quad (4)$$

Mansour et al. [3] use direct numerical simulation (DNS) data of forced turbulent channel flow to compute budgets for Reynolds stresses  $\overline{u'_i u'_j}$ . Besides the region very close to the wall, they find the diffusive transport due to pressure-velocity correlations indeed being smaller than that due to triple velocity correlations. Wörner and Grötzbach [4] [5] performed a series of direct numerical simulations of Rayleigh-Bénard convection in various fluids. From their results it appears that in this special type of convection not the triple correlation but the pressure correlation is the dominant term, both in equations 2 and 3. However, no physical explanation for this surprising result is given by the authors.

The objective of the present paper is twofold. First, we investigate whether the special relevance of diffusive transport by pressure fluctuations is a general feature of natural convection in horizontal fluid layers or not. Besides the Rayleigh-Bénard convection, we therefore analyse direct numerical simulations of another type of pure natural convection, this is the convection in an horizontal fluid layer which is internally heated by a volumetric heat source. As will be shown, the relative importance of pressure diffusion as compared to the triple correlation in this type of convection is much smaller than in the Rayleigh-Bénard case. The second objective is therefore to give a physical interpretation for the dominance of pressure correlations in turbulent diffusive transport in Rayleigh-Bénard convection.

## 2. DNS of Internally Heated Convection

### 2.1. Formulation of problem

The natural convection in a horizontal fluid layer of height  $D$  which is internally heated by a homogeneously distributed volumetric heat source  $q_v$  is of interest in several geophysical and technical systems. An example is reactor safety analysis in case of a hypothetical core melt down, see e.g. [6] [7] for a literature survey.

The important dimensionless groups which characterise the physical problem are the internal Rayleigh number  $Ra_I = g\beta q_v D^5 / (\nu\kappa\lambda)$  and the Prandtl number  $Pr = \nu/\kappa$ , where  $g$  = gravity,  $\beta$  = thermal expansion coefficient,  $\nu$  = kinematic viscosity,  $\kappa$  = thermal diffusivity, and  $\lambda$  = thermal conductivity. In the present study, the fluid Prandtl number is  $Pr = 7$  and the internal Rayleigh number ranges between  $5 \cdot 10^5 \leq Ra_I \leq 10^9$ .

Another important dimensionless number is the Damköhler number  $Da = q_v D^2 / (\lambda \Delta T_{max})$ , where  $\Delta T_{max}$  is the maximum temperature difference across the channel. As  $\Delta T_{max}$  is not known a priori for a given  $q_v$ , the same holds for  $Da$ . For fully developed convection, where  $q_v$  is completely removed across top and bottom wall, it follows by an energy balance that  $Da$  equals the sum of the Nusselt numbers, i.e.  $Da = Nu_{top} + Nu_{bottom}$ . Other dependent dimensionless numbers are the Grashof number  $Gr = Ra_I / (Pr \cdot Da)$  and the external Rayleigh number  $Ra_E = Ra_I / Da$ .

### 2.2. Numerical model

The direct numerical simulations are performed with the TURBIT code [8]. It is based on a finite volume method and solves the complete time-dependent three-dimensional conservation

Table 1: Parameter and grid data of the simulations:  $\Delta x_{1,2}$  = horizontal mesh widths (equidistant spacing),  $\Delta x_3$  = vertical mesh widths (non-equidistant spacing, W=wall),  $N_{1,2,3}$  = number of mesh cells.

$Pr$	$Ra_I$	$X_{1,2}$	$\Delta x_{1,2}$	$\Delta x_{3W,bottom}$	$\Delta x_{3,max}$	$\Delta x_{3W,top}$	$N_1$	$N_2$	$N_3$
7	$10^5$	6	0.1000	0.0370	0.069	0.0320	60	60	21
	$5 \cdot 10^5$	6	0.0750	0.0250	0.064	0.0190	80	80	27
	$10^6$	5	0.0625	0.0231	0.054	0.0161	80	80	31
	$5 \cdot 10^6$	5	0.0500	0.0228	0.049	0.0115	100	100	35
	$10^7$	5	0.0417	0.0180	0.036	0.0092	128	128	39
	$10^8$	4	0.0250	0.0120	0.026	0.0057	160	160	55
	$10^9$	3	0.0150	0.0061	0.019	0.0024	200	200	80
0.71	$Ra_E$ 630,000	7.92	0.0396	0.0050	0.037	0.0050	200	200	49

equations of mass, momentum, and energy. The Boussinesq approximation is employed, and the equations are solved in dimensionless form. For normalisation the channel height  $D$ , the velocity  $u_0 = \sqrt{g\beta\Delta T_0 D}$ , the pressure  $\rho u_0^2$ , and temperature difference  $\Delta T_0$  are used. The latter is related to a guess for the Damköhler number  $Da_0 = q_v D^2 / (\lambda \Delta T_0)$ , which needs to be specified at the begin of a simulation. Using the summation convention, the governing equations are given for a Cartesian coordinate system by:

$$\frac{\partial u_j}{\partial x_j} = 0 \quad (5)$$

$$\frac{\partial u_i}{\partial t} + \frac{\partial(u_i u_j)}{\partial x_j} = -\frac{\partial p}{\partial x_i} + \frac{1}{\sqrt{Gr_0}} \frac{\partial^2 u_i}{\partial x_j \partial x_j} - \delta_{i3}(T_{ref} - T) \quad (i = 1, 2, 3) \quad (6)$$

$$\frac{\partial T}{\partial t} + \frac{\partial(T u_j)}{\partial x_j} = \frac{1}{Pr \sqrt{Gr_0}} \left( \frac{\partial^2 T}{\partial x_j \partial x_j} + Da_0 \right). \quad (7)$$

The boundary conditions used are rigid upper and lower horizontal walls at  $x_3 = 0$  and  $x_3 = 1$ , respectively. For the simulations of the internally heated layer, both walls are isothermal and have equal temperature. In the horizontal directions  $x_{1,2}$  periodic boundary conditions with periodicity lengths  $X_{1,2}$  are applied. From an experimental point of view, this corresponds to the convection occurring in a container with large aspect-ratio.

Equations (5 - 7) are also valid for the Rayleigh-Bénard case. Since there is no heat generation in the fluid,  $q_v$  and  $Da_0$  are zero. The temperature difference  $\Delta T_0$  is that one between heated lower and cooled upper isothermal wall:  $\Delta T_0 = \Delta T_{max} = T_{Wall,bottom} - T_{Wall,top}$ .

In Table 1 we give the parameters and grid data of the simulations for the internally heated convection and for a recently refined simulation of Rayleigh-Bénard convection in air ( $Pr = 0.71$ ,  $Ra_E = 630,000$ ) [9]. We carefully ensured that the grids resolve the largest scales of convection and the smallest scales of turbulence and thus meet these indispensable requirements of the DNS method.

### 2.3. Verification

To verify the numerical results for the internally heated convection, the computed Nusselt numbers at top and bottom wall are compared with the experimental correlations of Jahn [10]

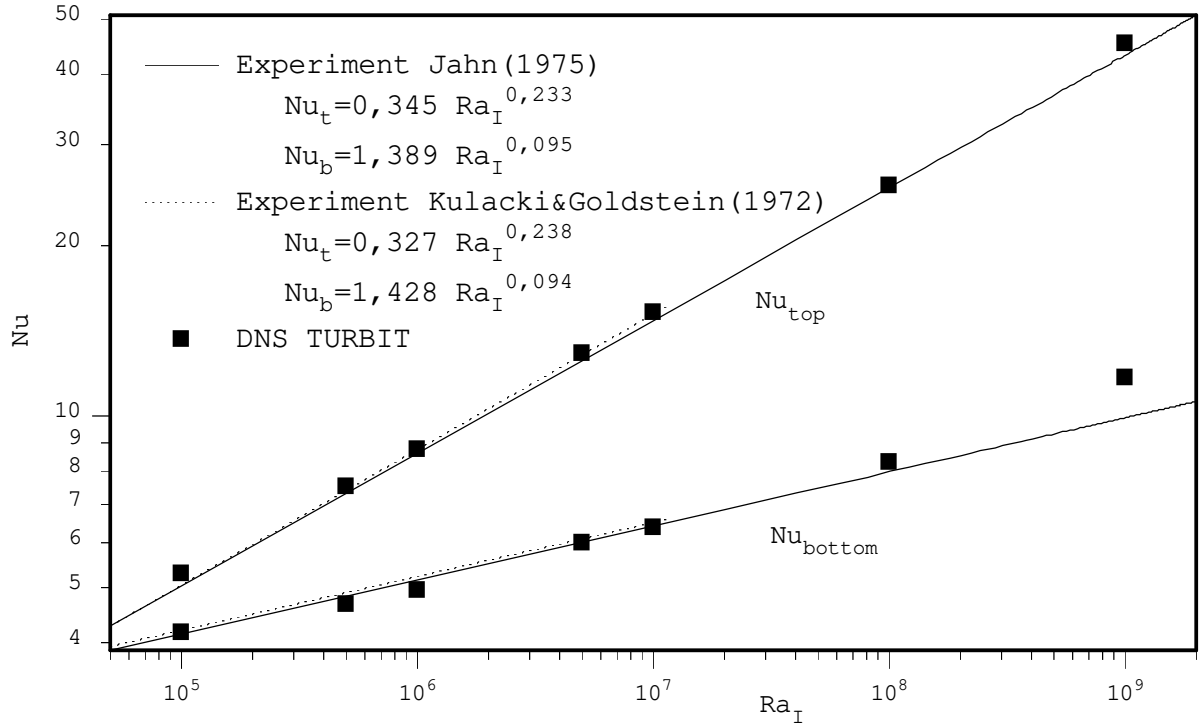


Figure 1: Comparison of computed Nusselt numbers at top and bottom wall with experimental correlations for internally heated convection.

and Kulacki & Goldstein [11], see Figure 1. Besides the simulation with  $Ra_I = 10^9$ , where the Nusselt number at the lower wall in the computation is little too high as compared to the correlation of Jahn [10], a very good agreement is achieved for the total heat transfer. For a more detailed verification of the simulations with  $Ra_I = 10^6$  and  $Ra_I = 10^7$  we refer to [12]. There, we also discuss the patterns and dynamics of the convection, whereas the present paper is limited to the analysis of turbulent diffusive transport of  $k$  and  $\overline{u_3' T'}$ .

### 3. Results for $D_{k,turb}$ and $D_{q_3,turb}$

#### 3.1. Case selection

For analysis of turbulent diffusive transport of  $k$  and  $\overline{u_3' T'}$  we focus for the internally heated layer on the simulation with  $Ra_I = 10^8$ . The Grashof number is about 407,000 and thus is comparable to the Rayleigh-Bénard case, where  $Gr \approx 887,000$ . The Grashof number is the relevant dimensionless number in the momentum equation (6). As  $Gr$  is of similar magnitude in both simulations, the turbulence level and thus velocity and pressure fields should be comparable, too. In the dimensionless energy equation (7), the relevant parameter is the Boussinesq number  $Bo = Pr^2 \cdot Gr$ . In the simulation with  $Ra_I = 10^8$  the value is  $Bo \approx 2 \cdot 10^7$ . This is about 50 times higher than in the Rayleigh-Bénard case, where  $Bo \approx 447,000$ . Thus, for the statistics of the temperature fields in both simulations we can not expect similarity.

#### 3.2. Evaluation of statistical data

Statistical quantities are evaluated from the DNS data by ensemble averaging over horizontal planes and additional time averaging. This procedure results in vertical profiles of averaged

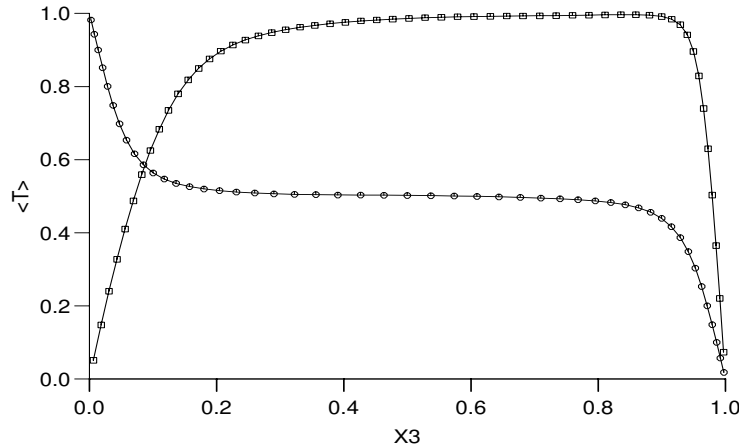


Figure 2: Vertical profile of mean temperature  $\langle T \rangle$ .  $\square$ : Internally heated convection ( $Pr = 7, Ra_I = 10^8$ ),  $\circ$ : Rayleigh-Bénard convection ( $Pr = 0.71, Ra_E = 630,000$ ).

quantities and is indicated by angled brackets, whereas the overbar denotes the conventional time averaging. Fluctuations with respect to  $\langle \Phi \rangle$  are denoted by  $\Phi''$ , and fluctuations with respect to  $\bar{\Phi}$  by  $\Phi'$ . For the geometries and boundary conditions used in the present DNS, statistical data are homogeneous with respect to the horizontal directions. Therefore, for fully developed turbulent flow both types of averages should be equivalent.

In Figure 2 we show evaluated profiles of mean temperature  $\langle T \rangle$ . The core region is almost isothermal, both, for the internally heated convection and for the Rayleigh-Bénard convection. In the Rayleigh-Bénard convection, both boundary layers near top and bottom wall are stratified thermally unstable. For the internally heated layer, there is a thin thermally unstable stratified boundary layer near the top wall and a thicker stably stratified one near the bottom wall.

### 3.3. Internally heated fluid layer

In Figure 3 we show vertical profiles of the correlations  $\langle u_3'' u_i'' u_i'' \rangle / 2$  and  $\langle u_3'' p'' \rangle$ , which cause according to equation (2) diffusive transport of  $k$  in vertical direction. With exception of the regions near bottom and top wall, the absolute value of the triple correlation of velocity fluctuations exceeds that of the pressure correlation. The same holds for the absolute values of the vertical gradient of both correlations.

Figure 4 gives profiles of correlations  $\langle T'' p'' \rangle$  and  $\langle u_3'' u_3'' T'' \rangle$ , which contribute to turbulent diffusive transport of vertical turbulent heat flux. In natural convection, fluctuations of temperature and vertical velocity are closely related, since the first ones induce buoyancy forces which drive the vertical motion. Thus, one should expect that the profiles of triple correlation and pressure correlation, respectively, in Figures 3 and 4 are similar. While this is partly true from a qualitative point of view, substantial differences are identified, too. Figure 4 shows that in the centre of the layer  $\langle T'' p'' \rangle$  is almost zero, whereas the triple correlation obeys an almost constant spatial gradient. Thus, in the centre of the layer diffusive transport of  $\overline{u_3' T'}$  is only due to the triple correlation. At the edges of the thermal boundary layers  $\langle T'' p'' \rangle$  shows peaks. Especially the one close to the upper wall is very sharp, indicating considerable pressure transport.

A comparison of the correlations given in Figures 3 and 4 for  $Ra_I = 10^8$  with those obtained for  $Ra_I = 10^9$  shows no major influence of the increase of the internal Rayleigh number. In

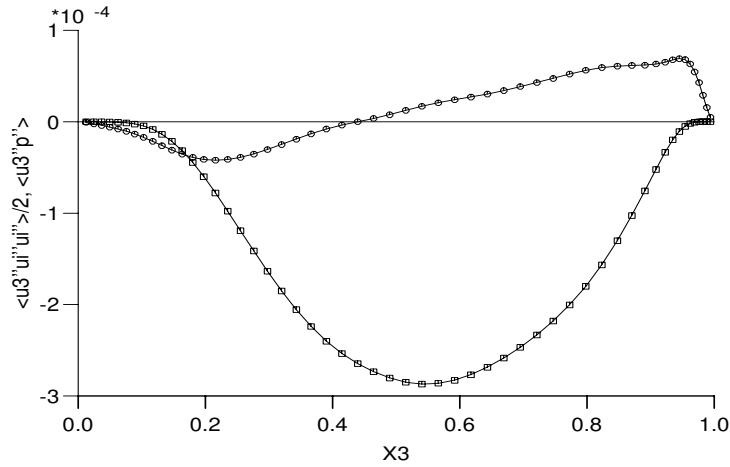


Figure 3: Internally heated convection ( $Ra_I = 10^8$ ).  $\square$  :  $\langle u_3''u_i''u_i'' \rangle / 2$ ,  $\circ$  :  $\langle u_3''p'' \rangle$ .

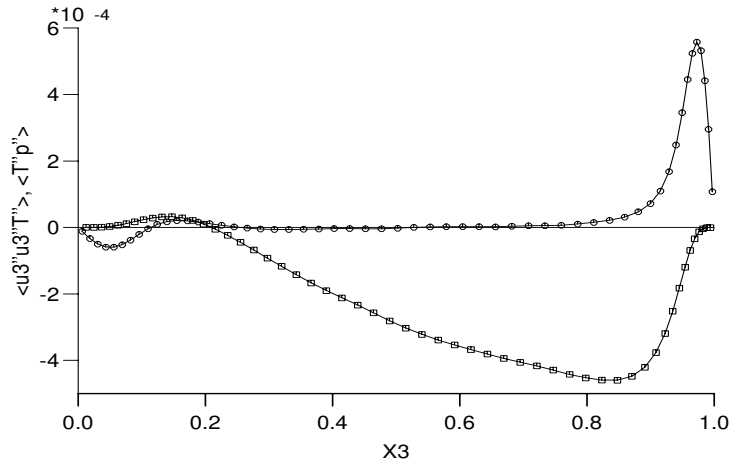


Figure 4: Internally heated convection ( $Ra_I = 10^8$ ).  $\square$  :  $\langle u_3''u_3''T'' \rangle$ ,  $\circ$  :  $\langle T''p'' \rangle$ .

accordance with the thinner boundary layers, for  $Ra_I = 10^9$  only a sharpening and shift of the peaks in the profile of  $\langle T''p'' \rangle$  towards the walls is observed.

### 3.4. Rayleigh-Bénard convection in air

As discussed in the introduction, from results of DNS of Rayleigh-Bénard convection in air and sodium at different Rayleigh numbers it is found that the pressure correlation represents the dominant turbulent transport term [4] [5]. See e.g. Figure 5, where profiles of  $\langle u_3''u_i''u_i'' \rangle / 2$  and  $\langle u_3''p'' \rangle$  are given for Rayleigh-Bénard convection in air. Furthermore, a remarkable similarity between both pressure correlations and both triple correlations in equations (2) and (3) is found. Compare  $\langle u_3''p'' \rangle$  in Figure 5 with  $\langle T''p'' \rangle$  in Figure 6, and  $\langle u_3''u_i''u_i'' \rangle / 2$  in Figure 5 with  $\langle u_3''u_3''T'' \rangle$  in Figure 6, respectively. For the triple correlations the similarity is striking, while the peaks in the profile of  $\langle T''p'' \rangle$  are more pronounced than in that of  $\langle u_3''p'' \rangle$ .

Thus, we find that in the Rayleigh-Bénard convection the turbulent diffusive transport of  $k$  and  $\overline{u_3'T'}$  is mainly due to pressure transport, whereas in the internally heated convection the

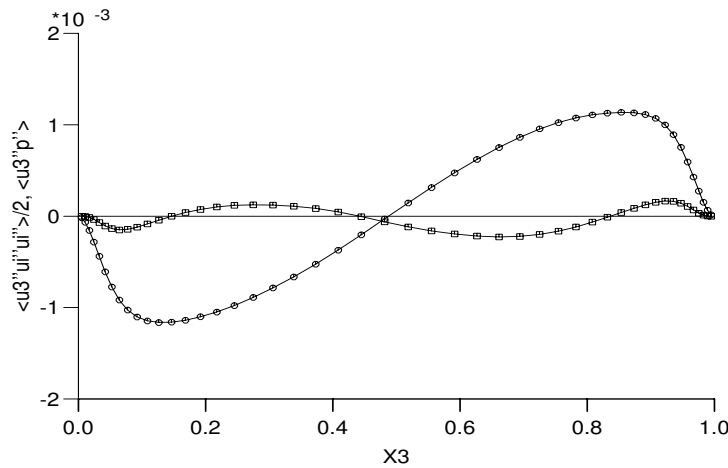


Figure 5: Rayleigh-Bénard convection in air ( $Ra_E = 630,000$ ).  $\square$  :  $\langle u_3'' u_i'' u_i'' \rangle / 2$ ,  $\circ$  :  $\langle u_3'' p'' \rangle$ .

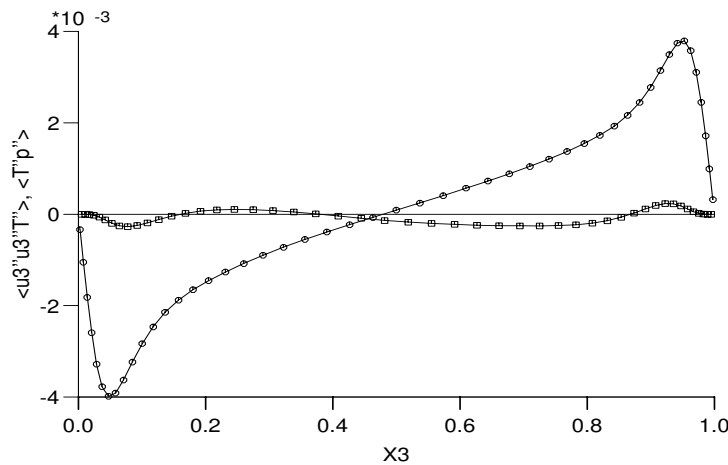


Figure 6: Rayleigh-Bénard convection in air ( $Ra_E = 630,000$ ).  $\square$  :  $\langle u_3'' u_3'' T'' \rangle$ ,  $\circ$  :  $\langle T'' p'' \rangle$ .

pressure transport is only of minor importance and the triple correlations in equations (2) and (3) represent the dominant terms. This result is quite surprising, since both physical problems under investigation are pure natural convection flows, taking place in the same geometrical configuration, and having quite similar boundary conditions. Therefore, in the next section we try to illuminate this phenomenon by analysing the transport mechanisms occurring in both convection layers.

## 4. Mechanisms of Pressure Transport

### 4.1. Rayleigh-Bénard convection in air

To illustrate the mechanism of heat transfer and the dynamics of Rayleigh-Bénard convection in air (see also [13]), we show the instantaneous isosurface for a dimensionless temperature value of  $T = 0.7$  (bottom wall:  $T = 1$ , upper wall:  $T = 0$ ), see Figure 7. The color code is for vertical velocity (red: upward flow, green:  $u_3 \approx 0$ , blue: downward flow). Hot fluid rises in plumes from the heated lower to the cooled upper wall. Near the lower wall the upward velocity

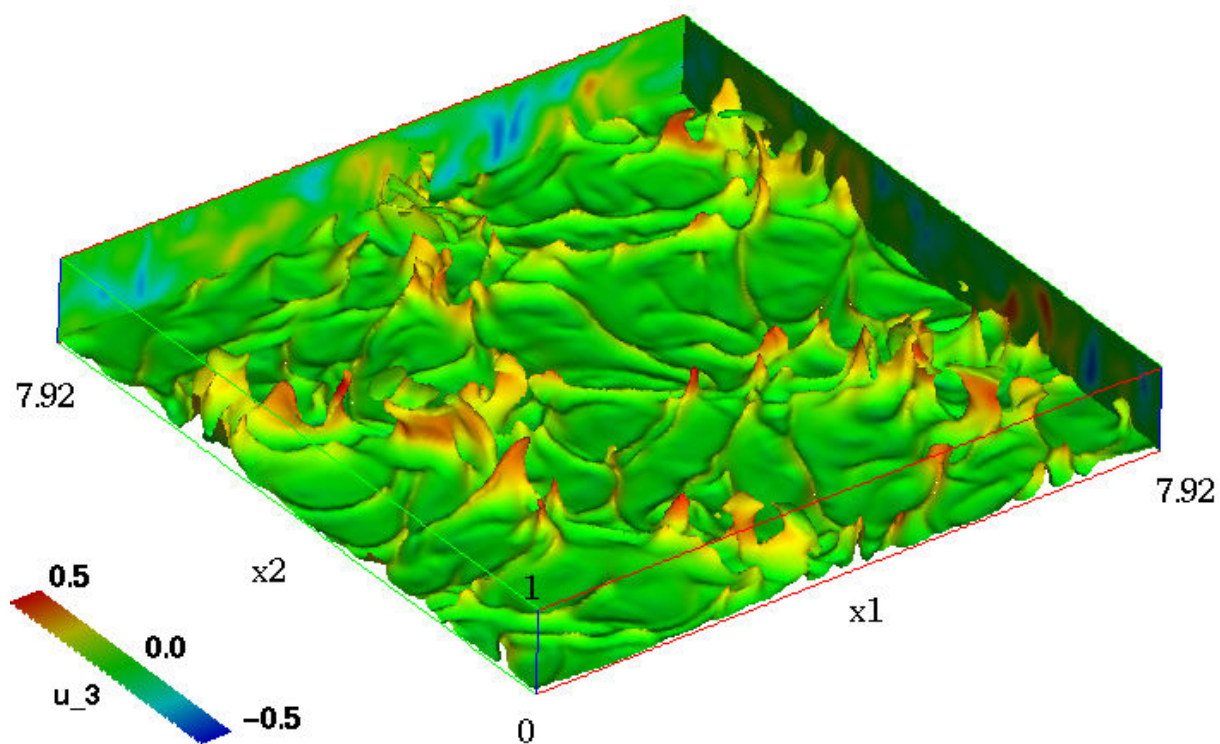


Figure 7: Rayleigh-Bénard convection in air ( $Ra_E = 630,000$ ). Isosurface for instantaneous temperature  $T = 0.7$  and color code for vertical velocity  $u_3$ .

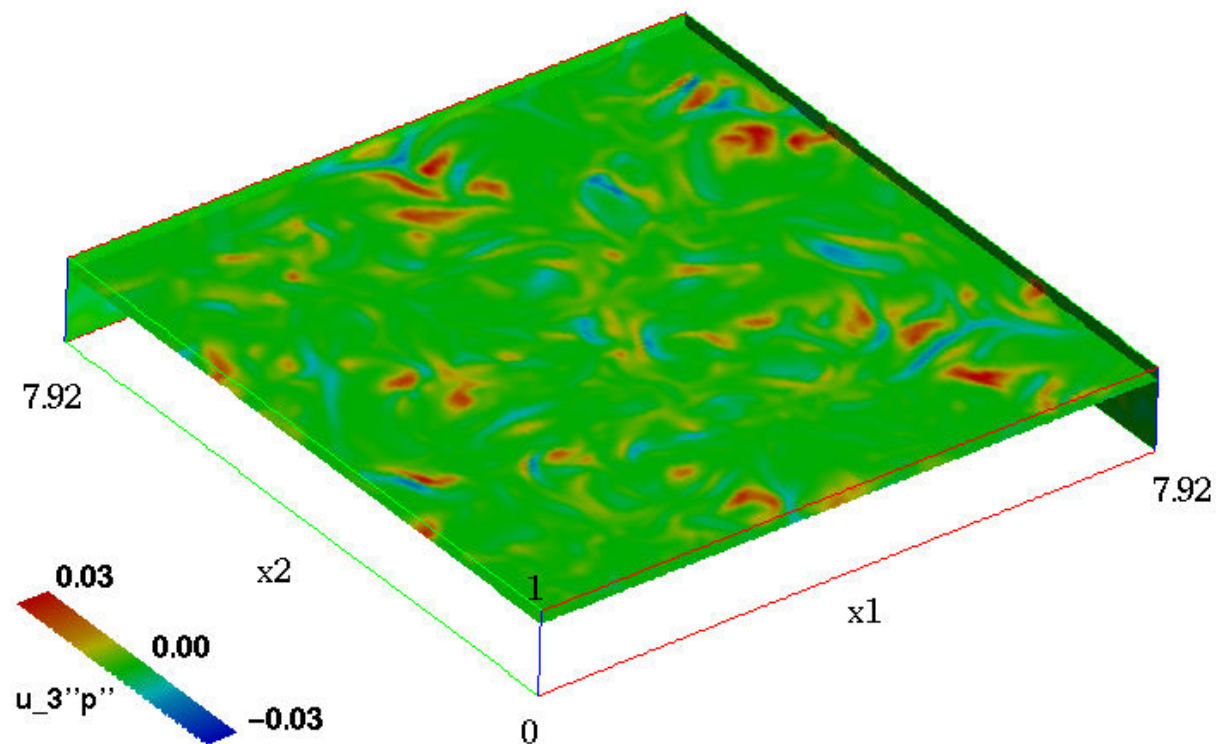


Figure 8: Rayleigh-Bénard convection in air ( $Ra_E = 630,000$ ). Instantaneous local values of  $u_3''p''$  in plane  $x_3 = 0.852$ .

of a rising hot plume is initially low. In the core region, it is accelerated by buoyancy forces and eventually penetrates the boundary layer at the upper wall with high kinetic energy. As Figure 7 shows, the plumes are concentrated in a few regions. In the boundary layer, these regions are connected by thin spoke patterns of slower upward movement. The dynamics of the flow involves two time scales. The generation and rise of plumes and the horizontal translation of spokes are fast processes, while a horizontal translation of the areas with concentrated plumes occurs only on a much larger timescale.

In Figure 8 we give a visualisation of the local value of correlation  $u_3''p''$  in plane  $x_3 = 0.852$ . From comparison of Figures 7 and 8 we find that near the top wall high positive values of  $u_3''p''$  occur at locations where hot plumes rise and penetrate the boundary layer at the upper wall. At such a location, the local values of  $u_3''$  and  $T''$  are positive. Since the vertical velocity of the rising plume is retarded as it approaches the upper wall, the local pressure increases, i.e.  $p'' > 0$ . Thus, the correlations  $u_3''p''$  and  $T''p''$  take locally high positive values. Averaging of  $u_3''p''$  over the horizontal plane results in  $\langle u_3''p'' \rangle > 0$  and also  $\langle T''p'' \rangle > 0$  in the upper half of the channel (see Figures 5 and 6). For the lower half of the channel, where cold plumes released from the top wall penetrate the boundary layer at the lower wall, the argumentation leading to  $\langle u_3''p'' \rangle < 0$  and  $\langle T''p'' \rangle < 0$  is equivalent.

#### 4.2. Internally heated convection

The dynamics of convection in an internally heated fluid layer is as well similar to that in Rayleigh-Bénard convection as it is different, too. Similar, because in both configurations there is an unstable thermal stratification at the top wall. This causes the Rayleigh-Taylor instability to generate cold plumes which leave the upper wall. In the Rayleigh-Bénard case, these downward falling plumes hit the boundary layer at the lower wall, which is stratified thermally unstable, too. In contrast, in the internally heated convection the thermal stratification of the quite thick boundary layer at the lower wall is stable (see Figure 2). The fluid in the lower part of the channel is therefore almost motionless. In the core region, cold plumes released from the top wall warm up. As they approach the boundary layer at the lower wall, their temperature is higher than that of the surrounding fluid. Thus, the orientation of buoyancy force is no longer downward, but has switched to upward direction. Since now buoyant and viscous forces counteract the downward directed inertial one, the falling plumes are slowed down smoothly. They penetrate the boundary layer at the lower wall with much less kinetic energy than it is the case in the Rayleigh-Bénard configuration. In the core and in the lower part of the internally heated layer, therefore correlations involving fluctuations of pressure are low. Since there are no plumes which rise from the bottom wall, one should expect that this also holds for the region close to the upper wall. Figure 4 however shows, that  $\langle T''p'' \rangle > 0$  takes a high positive value in the quite thin thermal boundary layer at the upper wall. A visualisation of local instantaneous correlation  $T''p''$  (similar to that in Figure 8 but not shown here) indicates that this result is due to sheets of cold (i.e.  $T'' < 0$ ) downward falling accelerated fluid (i.e.  $p'' < 0$ ). Neighbouring vertical sheets are connected. In a visualisation of  $T''p''$  in a horizontal plane close to the upper wall, this yields the well known characteristic network of irregular cells [8].

### 5. Conclusion

Direct numerical simulation data of Rayleigh-Bénard convection in air ( $Pr = 0.71$ ,  $Ra_E = 630,000$ ) and of internally heated convection ( $Pr = 7$ ,  $Ra_I = 10^8$ ) are used to investigate turbulent diffusive transport of turbulence kinetic energy and vertical turbulent heat flux. The results show that the dominance of pressure fluctuations in turbulent diffusive transport of  $k$

and  $\overline{u_3 T'}$ , found in earlier numerical studies for the Rayleigh-Bénard problem, is not a general feature of natural convection in horizontal fluid layers. It appears that the importance and efficiency of pressure transport is closely linked to the flow mechanisms and to the dynamics of the convective layers. Namely in the Rayleigh-Bénard case, the efficient pressure transport of turbulence kinetic energy and vertical turbulent heat flux is related to coherent structures (plumes), which are strongly intermittent.

In statistical turbulence models, closure assumptions are usually based on long-time averaged mean quantities (e.g. velocity or temperature). However, in turbulent Rayleigh-Bénard convection the long-time averaged mean velocity is zero, while on the time scale of the lifetime of coherent structures well defined mean values do exist. It is thus an open question whether statistical turbulence models based on long-time averaged mean values can at all yield reliable results for the flows under consideration.

## References

1. P. Bradshaw. Turbulence: the chief outstanding difficulty of our subject. *Experiments in Fluids*, 16:203-216, 1994.
2. J.L. Lumley. Computational modelling of turbulent flows. In *Advances in Applied Mechanics 18*, Ed.: C.-S. Yih, Academic Press, New York, pp. 123-176, 1978.
3. N.N. Mansour, J. Kim, and P. Moin. Reynolds-stress and dissipation rate budgets in a turbulent channel flow. *J. Fluid Mech.* 194:15-44, 1988.
4. M. Wörner and G. Grötzbach. Analysis of diffusion of turbulent kinetic energy by direct numerical simulations of natural convection in liquid metals. In *Proceedings NURETH-6*, Grenoble, France, Vol.1, pp. 186-193, 1993.
5. M. Wörner and G. Grötzbach. Turbulent heat flux balance for natural convection in air and sodium analysed by direct numerical simulations. In *Proc. 5th Int. Symp. on Refined Flow Modelling and Measurements*, Paris, France, pp. 335-342, 1993.
6. F.A. Kulacki and D.E. Richards. Natural convection in plane layers and cavities with volumetric energy sources. In *Natural Convection: Fundamentals and Applications*, Eds.: S. Kakac, W. Aung, and R. Viskanta, Springer , pp. 179-255 , 1985.
7. R.R. Nourgaliev and T.N. Dinh. Effect of Prandtl number on heat transfer characteristics in internally heated liquid pools with Rayleigh numbers up to  $10^{12}$ , *KTH Research Report KTH/NPS ND953*, Royal Institute of Technology, Stockholm, Sweden, 1995.
8. G. Grötzbach. Direct numerical and large eddy simulation of turbulent channel flows. In *Encyclopaedia of Fluid Mechanics*, Ed.: N.P. Cheremisinoff, Gulf Publ. Houston, Vol. 6, pp. 1337-1391, 1987.
9. M. Wörner and G. Grötzbach: DNS database of turbulent convection in horizontal fluid layers. [http://hbksun17.fzk.de:8080/IRS/eng/IRS3/TURBIT\\_DNS\\_database.html](http://hbksun17.fzk.de:8080/IRS/eng/IRS3/TURBIT_DNS_database.html).
10. M. Jahn. Holographische Untersuchung der freien Konvektion in einer Kernschmelze. Dissertation, TU Hannover, 1975.
11. F.A Kulacki and R.J. Goldstein. Thermal convection in a horizontal fluid layer with uniform volumetric energy sources. *J. Fluid Mech.*, 55:271-287, 1972.
12. M. Wörner, M. Schmidt, and G. Grötzbach. DNS of turbulence in an internally heated convective fluid layer and implications for statistical modelling. *IAHR Journal of Hydraulic Research*, special issue dedicated to Fluid Phenomena in Energy Exchanges, to appear.
13. G. Grötzbach: Direct numerical and large eddy simulation of turbulent heat transfer. In *Turbulence, Heat and Mass Transfer I*, Eds.: K. Hanjalić and J.C.F. Pereira, Begell House, pp. 25-39, 1995.